Supporting Information

Multivariate MOFs for Direct Writing of Alloy Nanoparticles

Ruiqian Ma[1], Haoqing Jiang[1], Chao Wang[1], Chengbin Zhao[1], Hexiang Deng*[, 1, 2]

[1]Key Laboratory of Biomedical Polymers-Ministry of Education, College of Chemistry and Molecular Sciences, Wuhan University, Wuhan 430072, China

[2]The Institute for Advanced Studies, Wuhan University, Wuhan 430072, China.

Section 1. Materials and experimental setup

Chemical reagent:

$Cu(NO_3)_2 \cdot 3H_2O$ (99.5 %), $Zn(NO_3)_2 \cdot 6H_2O$ (99.5 %), benzene-1,3,5-tricarboxylate (BTC, 99.5 %), ethanol (EtOH, 99.7%) were purchased from Sino pharm Chemical Reagent Co. Ltd., and directly used without further purification. Copper foil with thickness of 10 μm was purchased from Shenzhen Kejingstar Technology Co., Ltd. Pathological grade glass slides with dimension of 1×25×75 mm were bought from Citotest Labware Manufacturing Co., Ltd.

HKUST-1-Cu synthesis

HKUST-1-Cu was synthesized on the basis of conditions reported previously.[S1] Specifically, a solid mixture of $Cu(NO_3)_2 \cdot 3H_2O$ (400 mg, 1.66 mmol) and BTC (200 mg, 0.952 mmol) were dissolved in 12 ml solvent (DMF, EtOH and H_2O with volumetric ratio of 1:1:1) in a 23 ml vial. The vial was sealed and heated at 85 °C for 12 h to yield blue precipitate of HKUST-1-Cu. The unreacted BTC inside the pores of MOF was removed by extensive solvent exchange. Typically, MOF crystals were washed with DMF, during which the solvent was decanted and replenished 3 times (3×10 ml). EtOH was used to extract the DMF in pores of MOF, then the remaining EtOH was removed under vacuum overnight at room temperature and followed by vacuum at 150 °C to generate the activated HKUST-1-Cu sample.

HKUST-1-Zn synthesis

HKUST-1-Zn was synthesized by following the similar procedure of HKUST-1-Cu. Specifically, a solid mixture of $Zn(NO_3)_2 \cdot 6H_2O$ (493 mg,1.66 mmol) and BTC (200 mg, 0.952 mmol) were dissolved in 12 ml DMF in a 23 ml vial. The vial was sealed and heated at 85 °C for 16 h to yield white precipitate of HKUST-1-Zn. The unreacted BTC was removed by extensive DMF exchange, during which the solvent was decanted and replenished 3 times (3×10 ml). EtOH was used to extract the DMF in pores of MOF, then the remaining EtOH was removed under vacuum overnight at room temperature and followed by vacuum at 150 °C to generate the activated HKUST-1-Zn sample.

MTV-HKUST-1-CuZn synthesis

For the synthesis of MTV-HKUST-1, H_3BTC (200 mg, 0.95 mmol) was combined with 12 ml DMF and then placed into a 23 ml vial, the amount of each metal salts as well as their weight used in the starting reaction mixture are: for **-Cu89Zn11 -** $Cu(NO_3)_2 \cdot 3H_2O$ (160 mg, 0.66 mmol) and $Zn(NO_3)_2 \cdot 6H_2O$ (296 mg, 1.00 mmol); for **-Cu78Zn22 -** $Cu(NO_3)_2 \cdot 3H_2O$ (120 mg, 0.50 mmol) and $Zn(NO_3)_2 \cdot 6H_2O$ (345 mg, 1.16 mmol); for **-Cu67Zn3 -** $Cu(NO_3)_2 \cdot 3H_2O$ (80 mg, 0.33 mmol) and $Zn(NO_3)_2 \cdot 6H_2O$ (394 mg, 1.32mmol). Afterwards the vial were sealed in autoclaves and kept at 85 °C for 16h. The as-synthesized crystals were activated by solvent exchange followed by vacuum drying, which was the same with HKUST-1-Zn (Fig. S1A).

$Zn(NO_3)_2$-in-HKUST-1-Cu synthesis

Zinc nitrate in HKUST-1-Cu was synthesized by impregnation method. $Zn(NO_3)_2$-in-HKUST-1-Cu were obtained from 2 ml EtOH suspension of HKUST-1-Cu (110 mg, 0.5 mmol) and $Zn(NO_3)_2 \cdot 6H_2O$. The amount and weight of $Zn(NO_3)_2 \cdot 6H_2O$ used in the synthesis are: for **10%** - 6.5 mg (0.055 mmol); for **20% -** 37.1 mg (0.125 mmol); for **30% -** 63.6 mg (0.214 mmol). The mixture was followed by stirring overnight and vacuum degassing (Fig. S1C).

PM-HKUST-1 synthesis

Mixture of HKUST-1-Cu and HKUST-1-Zn was obtained by mixing these two activated MOFs up and followed by grinding.
PM-HKUST-1-Cu90Zn10, PM-HKUST-1-Cu80Zn20 and PM-HKUST-1-Cu70Zn30 were obtained by grinding the mixture of HKUST-1-Cu and HKUST-1-Zn at the ratio of 9:1, 8:2 and 7:3, respectively. (Fig. S1E).

MTV-HKUST-1-CuPd synthesis

For synthesis of MTV-HKUST-1-CuPd, H_3BTC (420 mg, 2.0 mmol) was combined with a mixture of $Cu(NO_3)_2 \cdot 3H_2O$ (609 mg, 2.50 mmol) and Pd(II) acetate (242 mg, 1.08 mmol) and then placed into a 23 ml vessel. Subsequently 15ml of H_2O/ EtOH (1:1) solution was added. Afterwards the vessel was sealed in autoclaves and kept at 75 °C for 12h. The as-synthesized crystals were activated by solvent exchange followed by vacuum drying.

Section 2. Laser patterning procedure

a) **Sample preparation.** In general, 15 mg of activated MOF powder was placed in a circular hole (19 mm in diameter) of copper foil on glass substrate. Another glass was placed on the top of the MOF powder to evenly spread it across the cavity. At last, the two glass sides were fixed by scotch tape to closely packed the MOF powder.

b) **Laser system setup.** A nanosecond pulse fiber laser (YLP-0.5-80-10, IPG photonics) was used as laser source. The pulse duration of the laser was 80 ns and operated at wavelength of 1064 nm at 20-200 kHz. The output laser power could be tuned from 1 to 10 w accordingly. The output laser power was carefully calibrated by an optical power meter (OPHIR). A set of galvanomirror (6240H, Cambridge Technology Inc.) and F-Theta lens (F-Theta-Ronar, LINOS) were served for beam scribing and focusing, respectively.

c) **The nano-LaMP procedure.** In a typical nano-LaMP process, the prepared sample from a) was placed on a XYZ stage (Suruga Seiki) and the focal length was carefully adjusted to produce 50 μm spot size on MOF layer. The laser scribing patterns could be predesigned in software and realized by the galvanometers. The power of laser was adjusted at 3.5 w and the scanning speed was 75 mm s^{-1}. After laser scribing, alloy nanoparticles were instantly deposited with metallic luster on the upper glass. The glass with alloy patterns were washed with water, sonicated in ethanol and dried in air before further characterization.

Section 3. Sample characterization

The as synthesized MOF crystals were polyhedral crystals with size around 30 μm (Fig. S1B, Fig. S1D, Fig. S1F, Fig. S7). We use PXRD to confirm the phase purity of these crystals. PXRD data was recorded on a Rigaku Smartlab 9 kW diffractometer, in parallel beam geometry employing Cu Kα lines focused radiation (λ = 1.5406 Å) at 45 kV, 200 mA with a scan speed of 1º/min and a step size of 0.01º in 2θ at ambient temperature and pressure. Simulated PXRD patterns were calculated using Mercury 3.0 software from the single crystal data. PXRD pattern of the synthesized MOF matched well with the simulated one (Fig. S4A and S5A), confirming the phase purity of the MOF sample. The light absorptivity of these precursors was confirmed by Uv-Vis absorption spectrum. The absorption of HKUST-1-Cu, HKUST-1-Zn, 30% $Zn(NO_3)_2$-in-HKUST-1-Cu, MTV-HKUST-1-Cu67Zn33 and $Zn(NO_3)_2 \cdot 6H_2O$ at 1064 nm were 69%, 25%, 77%, 70% and 29%, respectively (Fig. S3). The results revealed the light absorptivity of all kinds of MOF precursors in this study at the wavelength of laser (1064 nm). It was clear that MTV-MOF exhibited high light adsorption, thus guaranteed the efficient and conversion to alloy nanoparticles.

To confirm the successful formation of the MTV-HKUST-1, high resolution X-ray photoelectron spectroscopy (XPS) was performed on ESCALAB 250Xi (Thermo Fisher) with Al Kα as excitation source. We also tested the XPS spectra of HKUST-1-Cu and HKUST-1-Zn crystals as a comparison (Fig. S6). Two main peaks at binding energy of 1021.8 and 1044.9 eV were found in Zn 2p spectra of MTV-HKUST-1-Cu67Zn33, corresponding the Zn $2p_{3/2}$ and Zn $2p_{1/2}$, respectively. In contrast, Zn 2p spectra of the HKUST-1-Zn showed main peaks at 1022 and 1045.1 eV, which was different from Zn in MTV-HKUST-1. Cu 2p spectra of MTV-MOF show obvious peaks at 934.7 and 954.6 eV, which are same with Cu 2p in HKUST-1-Cu. However, the Cu $2p_{3/2}$ of MTV-HKUST-1 has a split peak at 932.8 eV, while the Cu $2p_{3/2}$ split peak of HKUST-1-Cu is showed at 933 eV. Moreover, characteristic peak of Cu^{2+} at 571.3 eV in the Cu LMM auger spectra of MTV-HKUST-1 was also observed, while the peak of HKUST-1-Cu is showed at 571.6 eV. The XPS spectra results indicate the successful formation of MTV-HKUST-1.

N_2 adsorption isotherm were measured on a Quantachrome Autosorb-1 automatic volumetric instrument. A liquid nitrogen bath (77 K) was used for isotherm measurements. Ultra-high purity grade (99.999 %) N_2 was used for adsorption test. The BET analysis is performed by plotting $x/v(1 - x)$ vs x, where $x = P/P_0$ (P_0 = 1 bar) and v is the volume of nitrogen adsorbed per gram of MOF at STP. This analysis produces a curve typically consisting of three regions: concave to the x axis at low pressures, linear at intermediate pressures, and convex to the x axis at high pressures. The slope ($[c - 1]/v_m c$) and y intercept ($1/v_m c$) of this linear region give the monolayer capacity, v_m, that is then used to calculate the surface area from $A = v_m \sigma_0 N_{AV}$, where σ0 is the cross-sectional area of the adsorbate at liquid density (16.2 $Å^2$ for nitrogen) and N_{AV} is Avogadro's number. HKUST-1 and its homologs show typical type I isotherm (Fig.

S4B and S5B), suggesting the microporous nature. BET surface area of 10%, 20% and 30% $Zn(NO_3)_2$-in-HKUST-1-Cu were calculated to be 766, 12 and 4 m^2 g^{-1}, respectively, while those of the MTV-HKUST-1 were 1713, 1703 and 1695 m^2 g^{-1} (Fig. S4B and Table S1), based on non-local density functional theory (NLDFT) using a carbon model containing cylindrical pores. The surface area of HKUST-1-Cu was in accordance with reported value, suggesting successful activation of the MOF. After dried under vacuum and removed guest molecules, the surface of HKUST-1-Zn collapsed, leaving only small pores at the surface. And the complete collapse of large pores at the surface effectively inhibits N_2 gas from entering the bulk structure. Therefore, HKUST-1-Zn showed no N_2 adsorption.

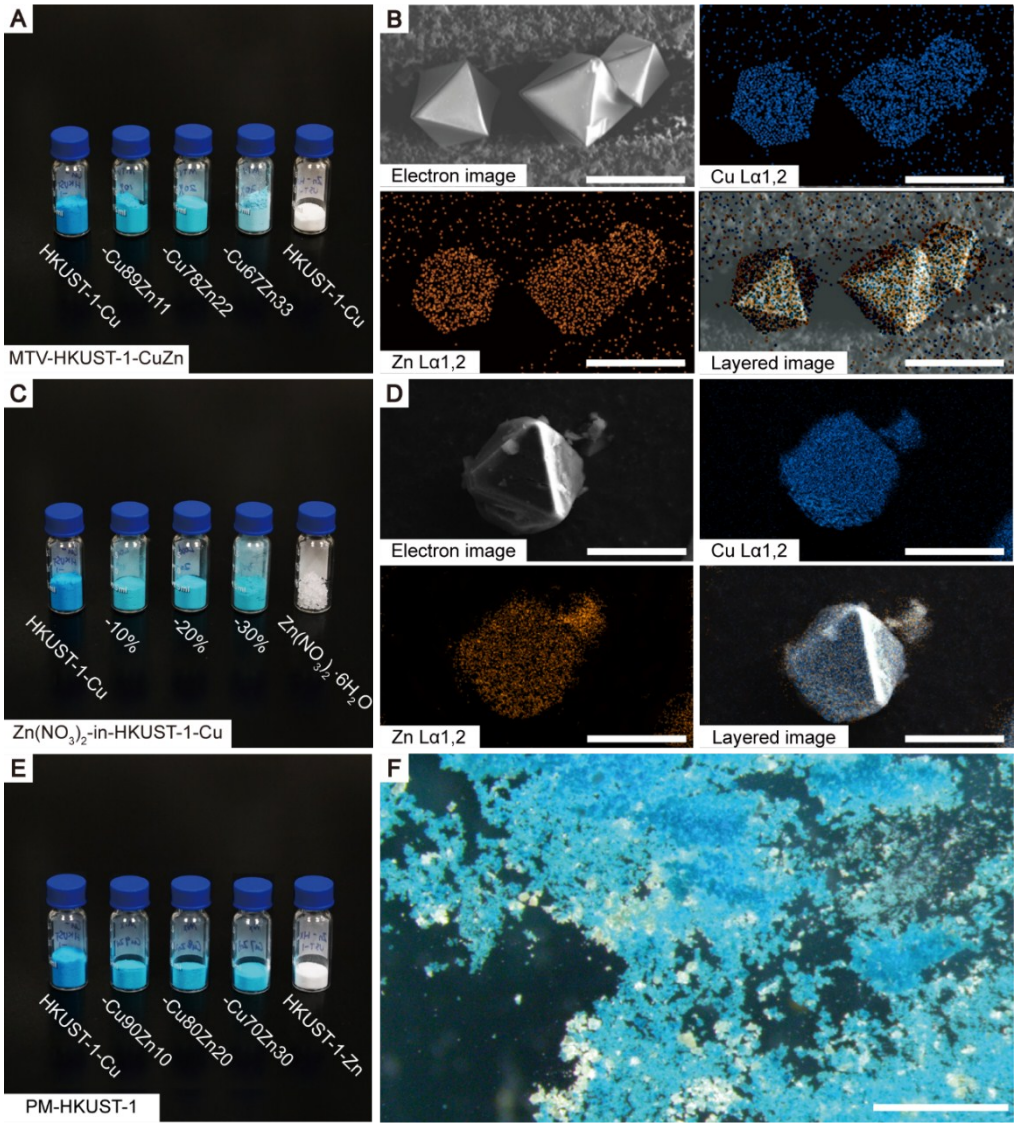

Figure S1. Optical images of MOF precursors: (A) MTV-HKUST-1, (C) $Zn(NO_3)_2$-in-HKUST-1-Cu, and (E) PM-HKUST-1, respectively. (B) The SEM image and elemental mapping of Cu, Zn and their mixture in MTV-HKUST-1-Cu67Zn33. (D) The SEM image and elemental mapping of Cu, Zn and their mixture in 10%$Zn(NO_3)_2$-in-HKUST-1-Cu. (F) Optical image of PM-HKUST-1-Cu70Zn30. The scale bars are (B) 50 µm, (D) 25 µm, (F) 1 mm.

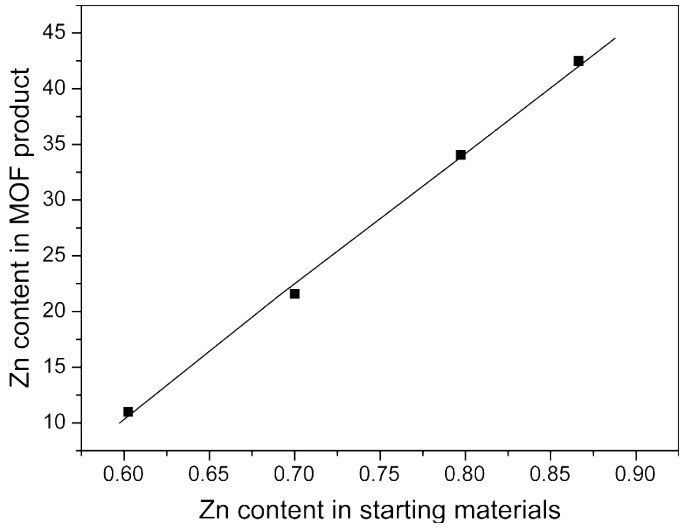

Figure S2. Standard curve between the stoichiometry of start materials and the product of MTV-HKUST-1-CuZn.

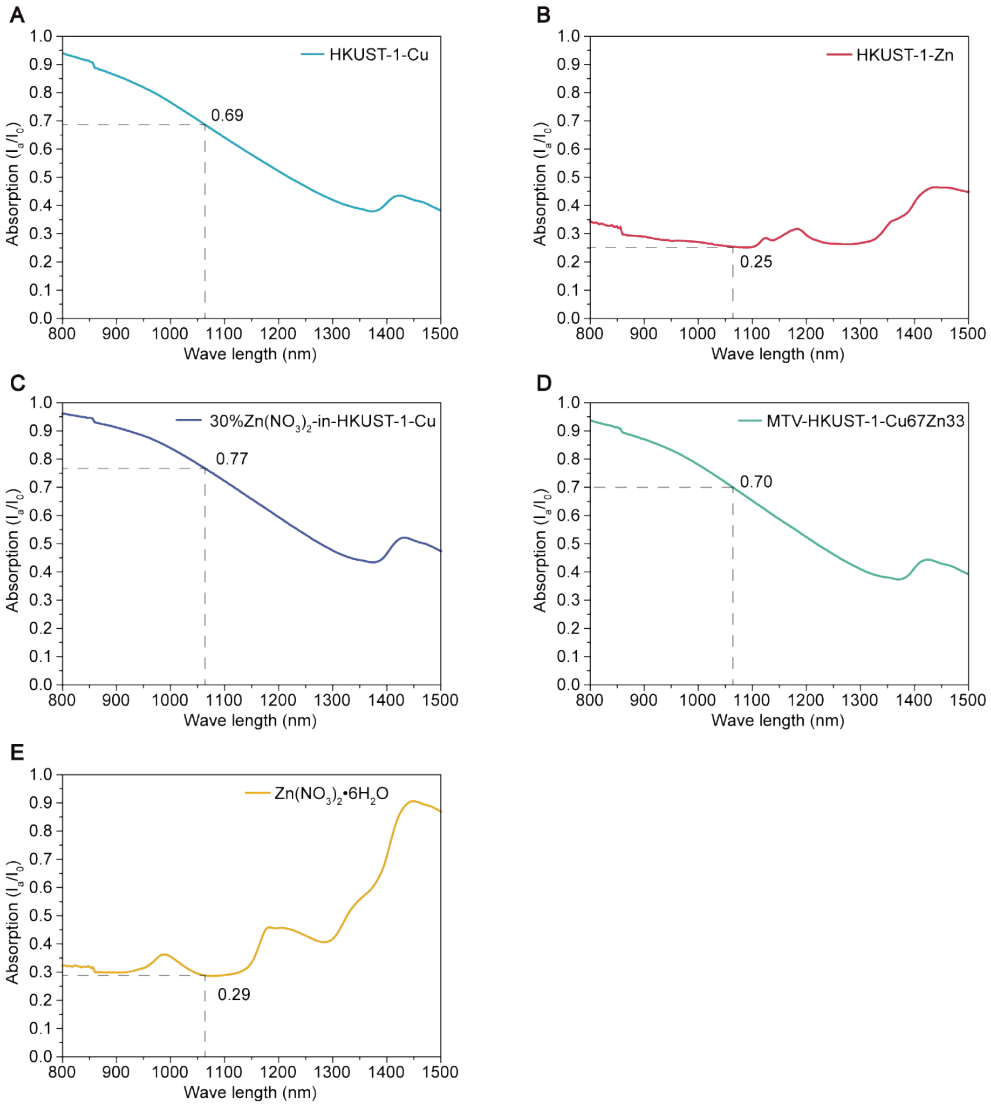

Figure S3. Light absorption spectrums of (A) HKUST-1-Cu, (B) HKUST-1-Zn, (C) 30%$Zn(NO_3)_2$-in-HKUST-1-Cu, (D) MTV-HKUST-1-Cu67Zn33 and (E) $Zn(NO_3)_2 \cdot 6H_2O$, respectively.

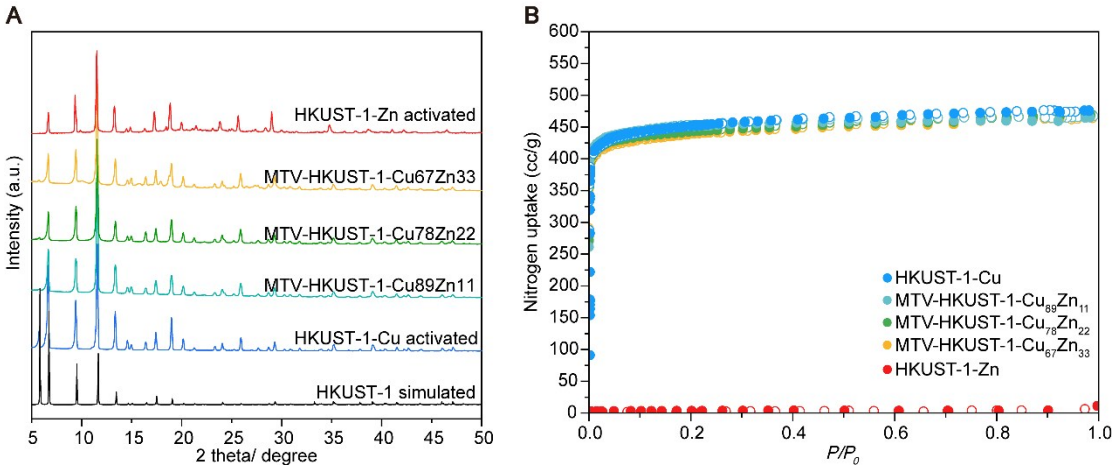

Figure S4. (A) PXRD images and (B) N_2 adsorption of HKUST-1-Cu and MTV-HKUST-1.

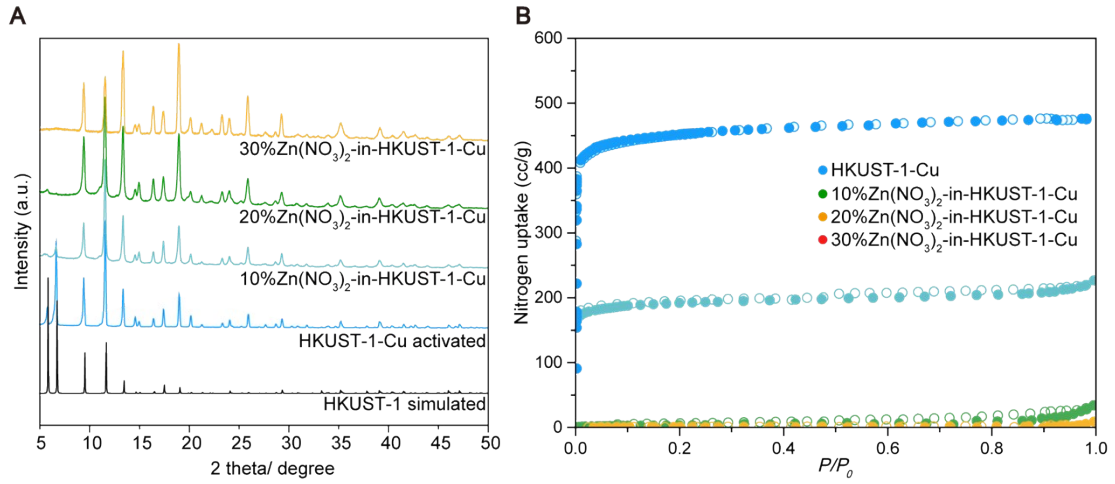

Figure S5. (A) PXRD images and (B) N_2 adsorption of HKUST-1-Cu and $Zn(NO_3)_2$-in-HKUST-1- Cu.

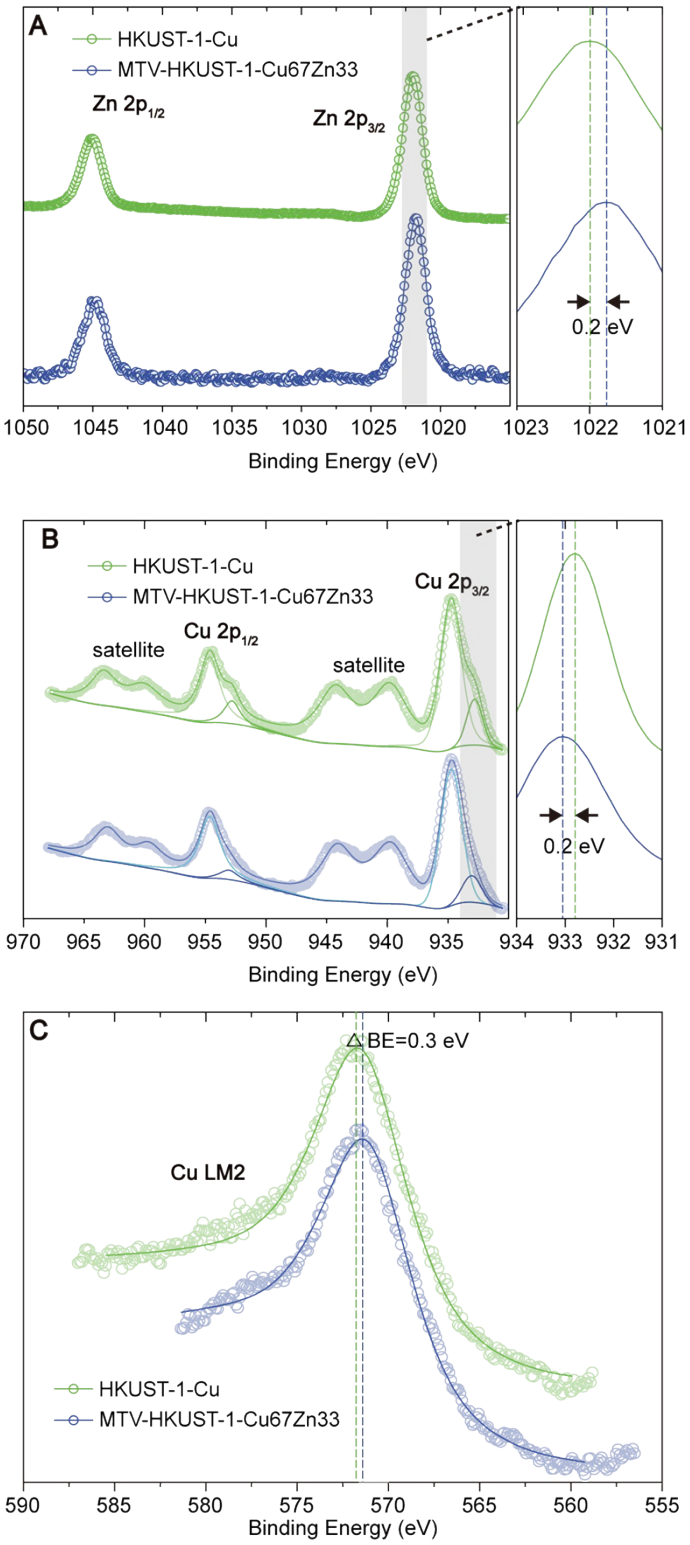

Figure S6. (A, B) XPS overlay of MTV-HKUST-1-Cu67Zn33 with its single component counterparts, HKUST-1-Zn and HKUST-1-Cu. (C) Cu Auger spectra of MTV-HKUST-1-Cu67Zn33 and HKUST-1-Cu.

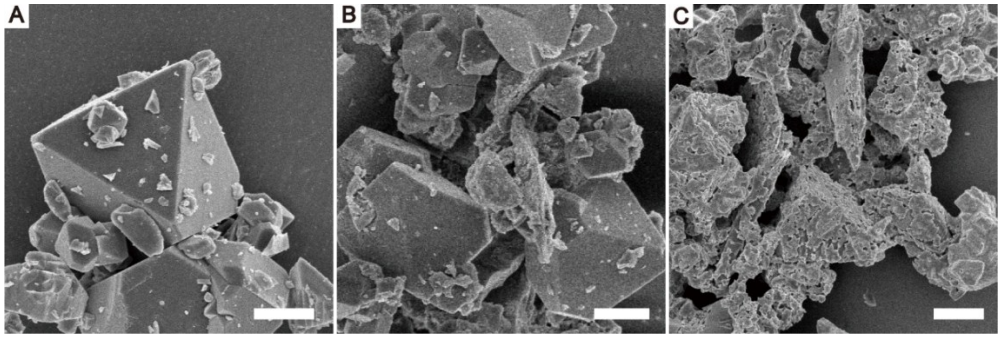

Figure S7. SEM images of (A) 10%, (B) 20% and (C) 30%$Zn(NO_3)_2$-in-HKUST-1-Cu, respectively. The scale bar is 10 μm.

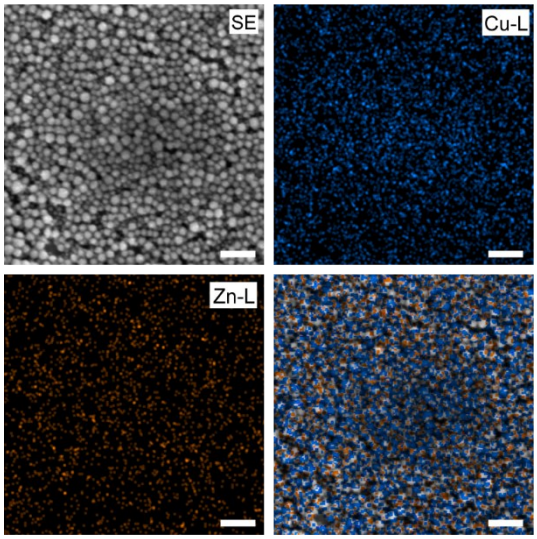

Figure S8. SEM and EDS images of Cu-Zn alloy nanoparticles produced by MTV-HKUST-1-Cu78Zn22. The scale bar is 100 nm.

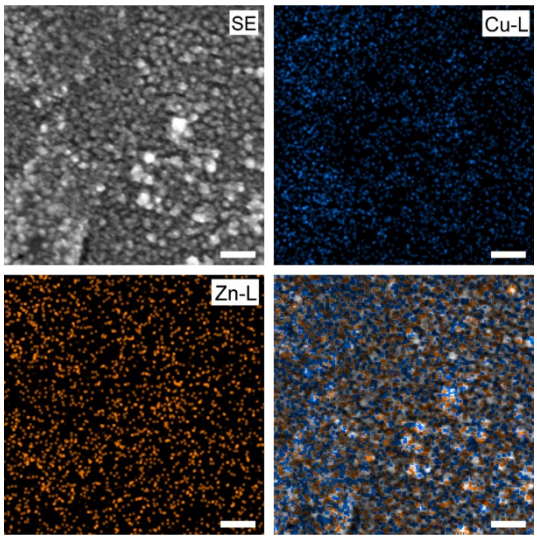

Figure S9. SEM and EDS images of Cu-Zn alloy nanoparticles produced by 20%$Zn(NO_3)_2$-in-HKUST-1-Cu. The scale bar is 100 nm.

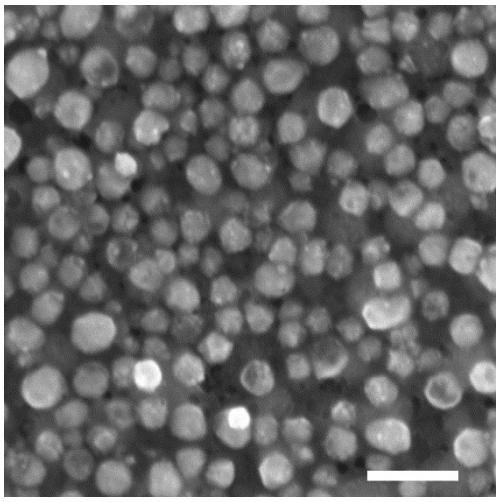

Figure S10. Zn nanoparticles produced by Zn-HKUST-1 after laser irradiation (scale bar: 100 nm).

Figure S11. EDS maps of deposition produced by physical mixture of pure HKUST-1-Cu and -Zn.

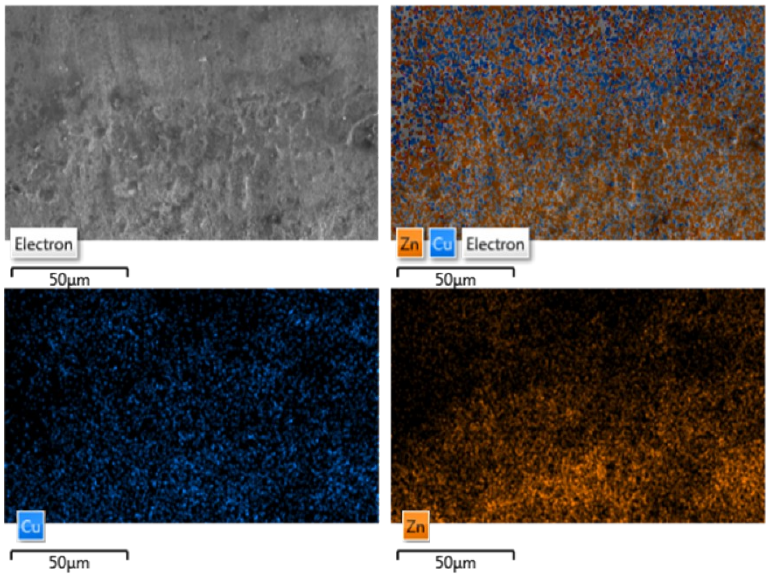

The resulting pattern was composed of Cu nanoparticles-rich domains and Zn nanoparticles-rich domains.

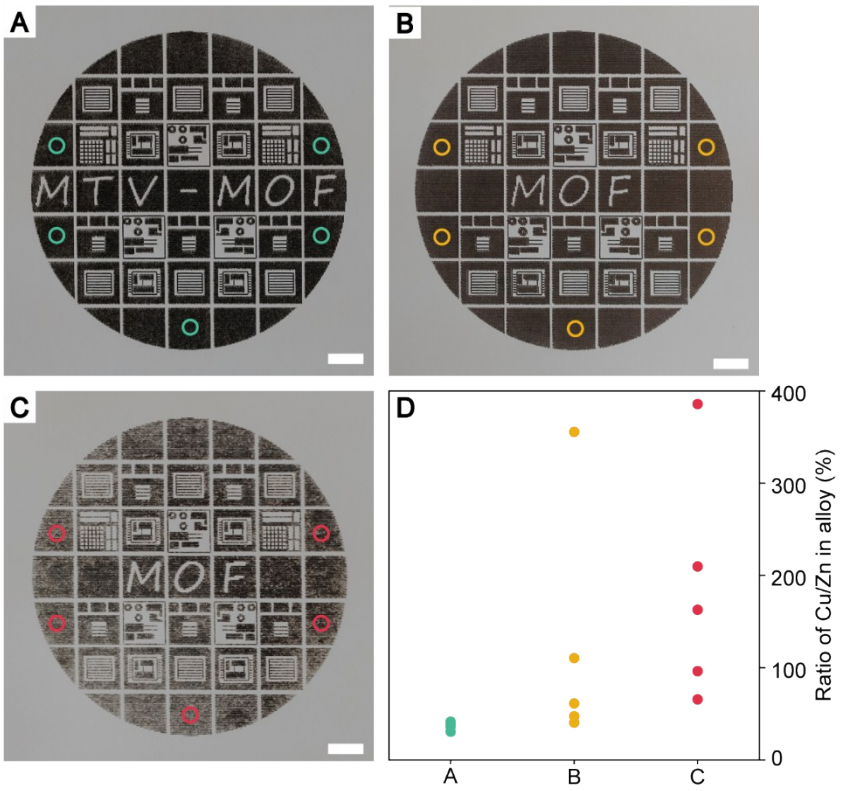

Figure S12. The optical images of the coating fabricated by nano-LaMP using (A) MTV-HKUST-1-Cu78Zn22, (B) 20%$Zn(NO_3)_2$-in-HKUST-1 and (C) PM-HKUST-1-Cu80Zn20, respectively. (D) The atomic ratio of Cu to Zn in coating revealed by EDX. The scale bar is 2 mm.

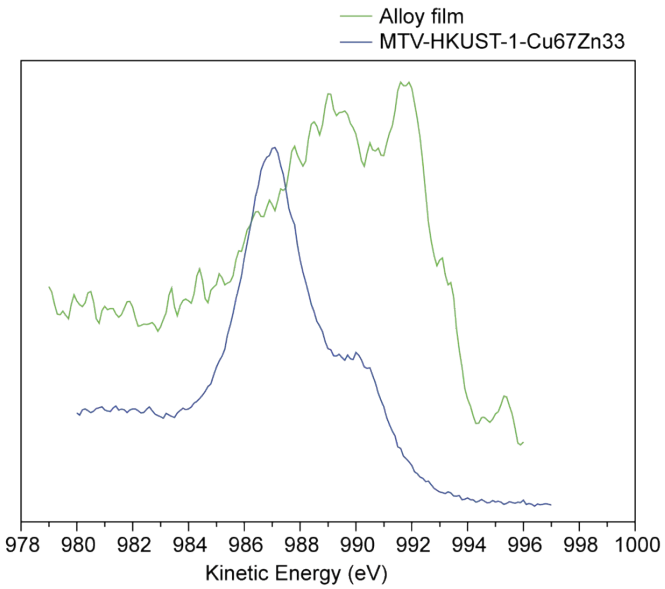

Figure S13. Zn LMM Auger spectra of alloy film and MTV-HKUST-1-Cu67Zn33.

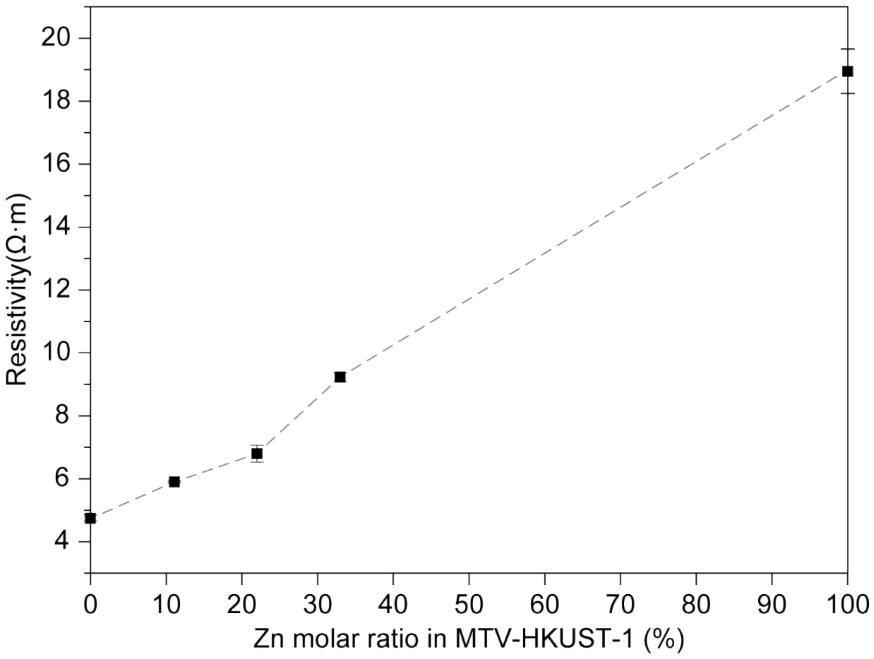

Figure S14. The resistivity of metal or alloy film produced by MOF.

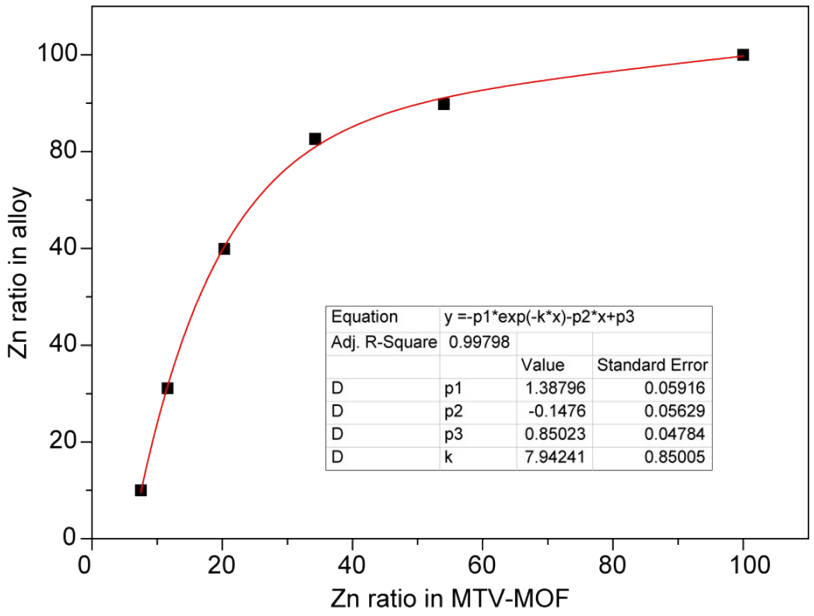

Figure S15. The correspondence of Zn ratio in MTV-HKUST-1 and alloy.

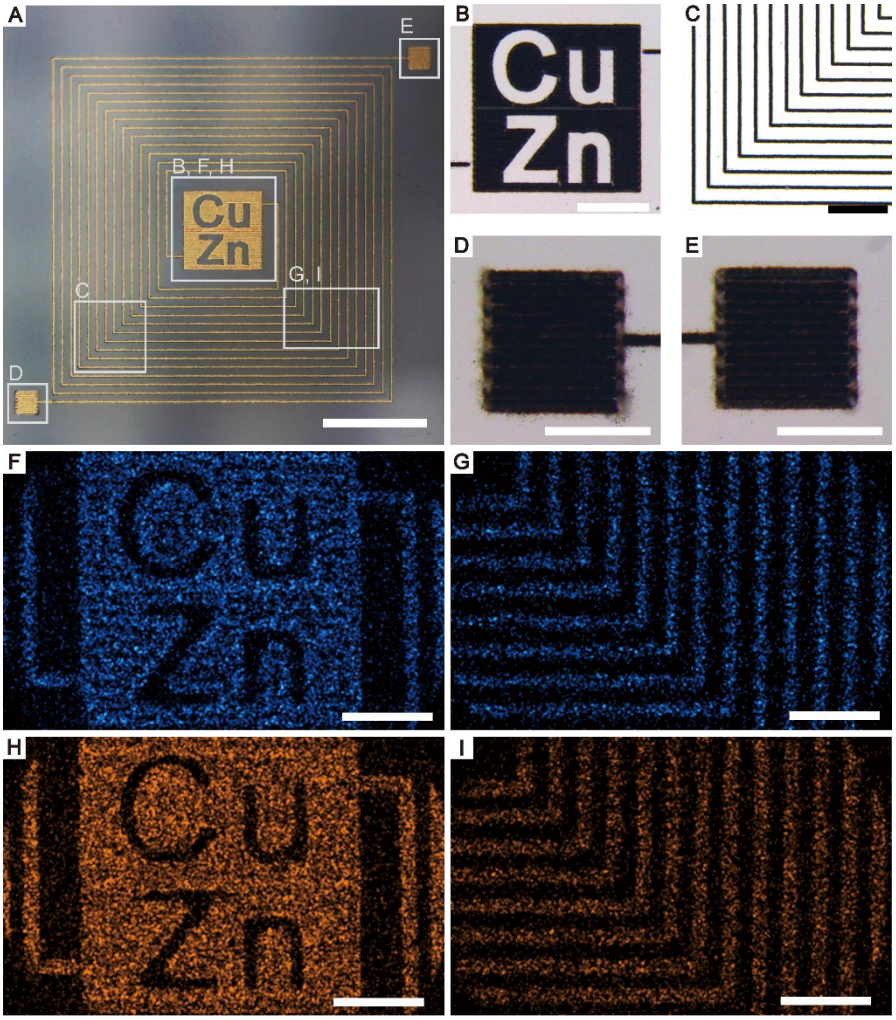

Figure S16. The Cu- Zn alloy based coil pattern fabricated by laser metallurgy using MTV-HKUST-1-Cu78Zn22. (A, B, C, D, E) Optical images of the coil. (F, G, H, I) Elemental mapping of Cu and Zn. The scale bars are (A) 3mm, (B, C) 2 mm, (D, E) 1 mm, (F-I) 500 μm.

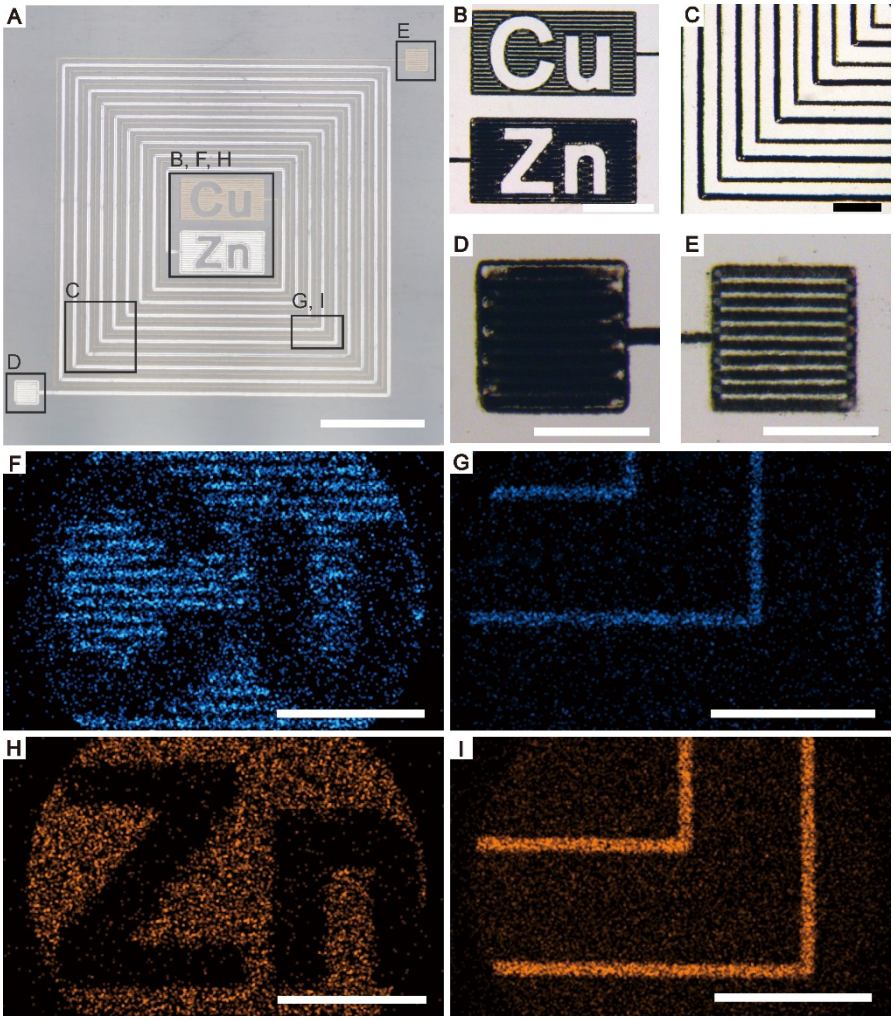

Figure S17. The Cu and Zn based coil pattern fabricated by laser metallurgy using HKUST-1-Cu and HKUST-1-Cu individually. (A, B, C, D, E) Optical images of the coil. (F, G, H, I) Elemental mapping of Cu and Zn. The scale bars are (A) 3 mm, (B) 2 mm, (C-E) 1 mm, (F-I) 500 μm.

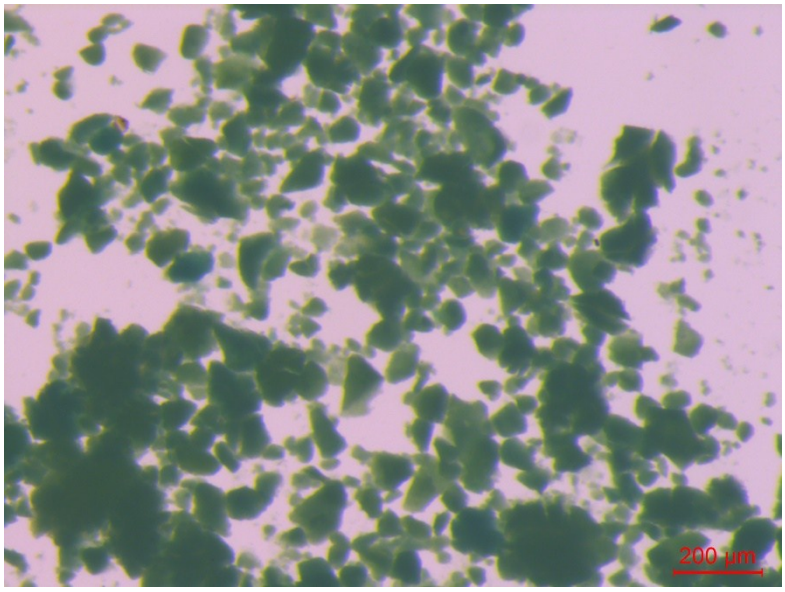

Figure S18. Optical image of MTV-HKUST-1-CuPd.

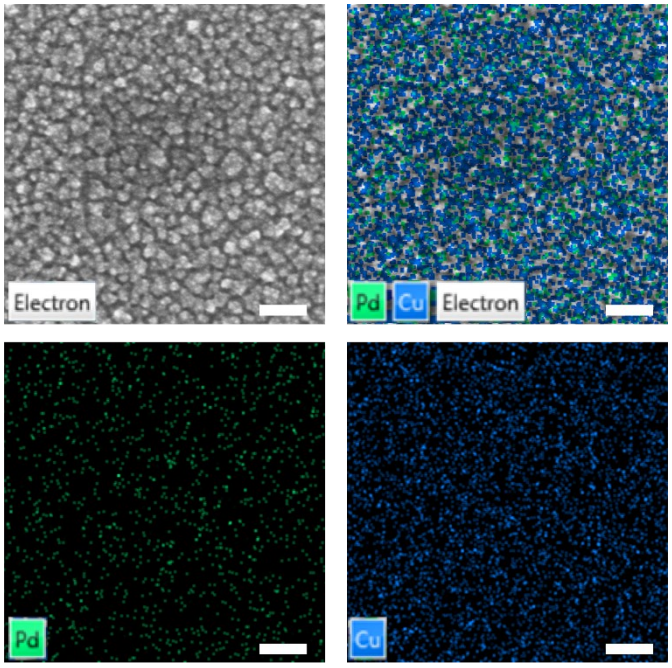

Figure S19. SEM and EDS images of Cu-Pd alloy nanoparticles produced by MTV-HKUST-1-CuPd. The scale bar is 50 nm.

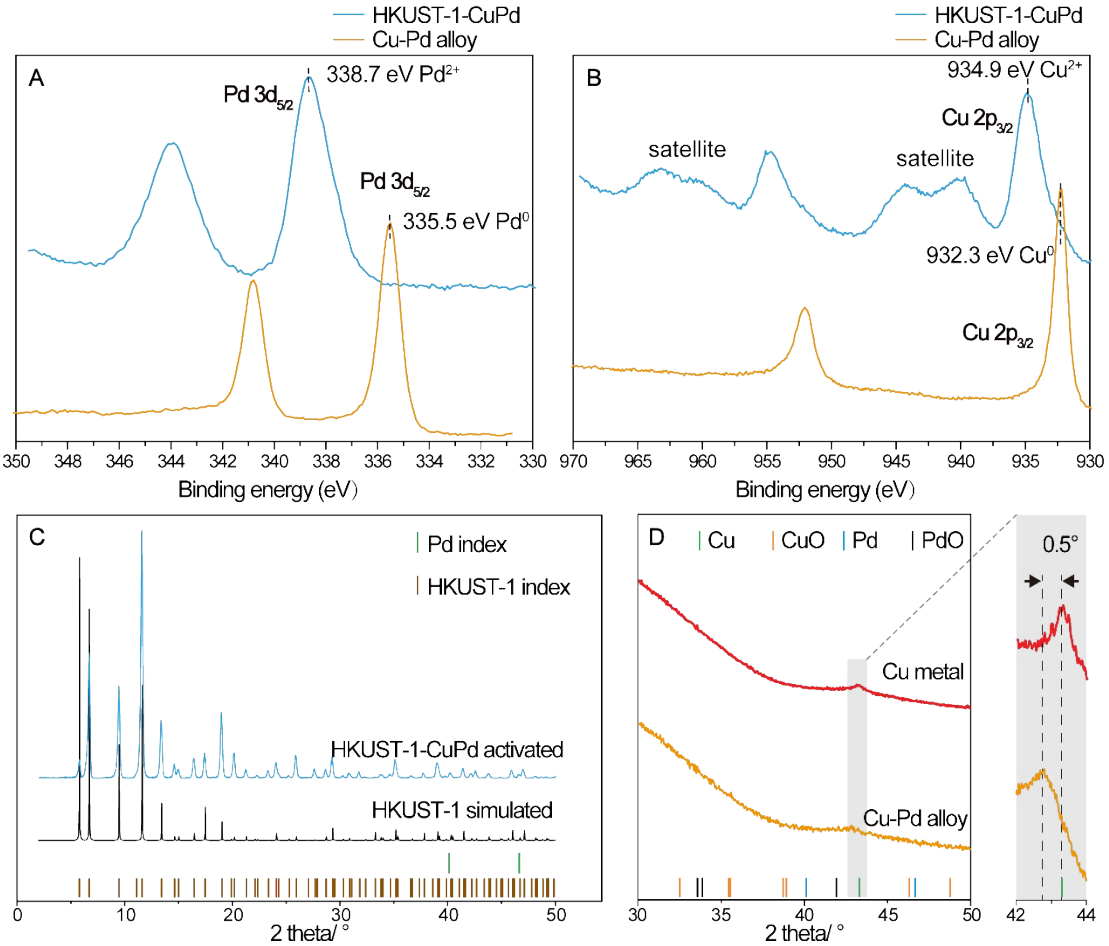

Figure S20. (A, B) XPS patterns of Cu-Pd alloy nanoparticles and the corresponding MTV-HKUST-1-CuPd. PXRD pattern of (C) MTV-HKUST-1-CuPd and (D) the corresponding Cu-Pd alloy in comparison with Cu metal produced by HKUST-1-Cu.

Section 4. Alloy nanoparticles application

The electrode was fabricated using nano-LaMP on MTV-HKUST-1-CuZn after replacement of ordinary glass by ITO glass. The resulting Cu-Zn alloy nanoparticle electrode was calcined in air for 2 h at 500 ℃ to remove the residual carbon on the ITO glass and oxidize the Cu-Zn alloy nanoparticles to form $Cu_{1-x}Zn_xO$ nanoparticles. Cyclic voltammetry (CV) was used to study the electrocatalysis of glucose oxidation at electrode within the potential range from 0 to 0.9 V (Fig. S21). The absence of redox peak in the control experiment using pure ITO glass alone. Therefore, the redox behavior in the electrode prepared from MOFs can be attributed to $Cu_{1-x}Zn_xO$ nanoparticles in the electrode.

Amperometric method was performed for the oxidation of glucose. Fig. S22 shows that the steady-state current response of glucose oxidation on $Cu_{1-x}Zn_xO$ nanoparticle electrode at +0.75 V, with different concentrations of 50, 100, 500, 1000, 10000 μM of glucose added into continuously stirred 0.1 M NaOH. The inset of Fig. S22 also describes that i–t current response of glucose with low concentrations such as 0.2, 1 and 5 μM. The steady-state current was increased while adding each injection of glucose concentration. This result reveals that the $Cu_{1-x}Zn_xO$ nanoparticle electrode has favorable electrocatalytic behavior toward glucose. The calibration plot shows the linearity between the current and glucose concentration (Fig. S23). The current was increased with increasing the glucose concentration with the linear range from 0.2 to 2000 μM.

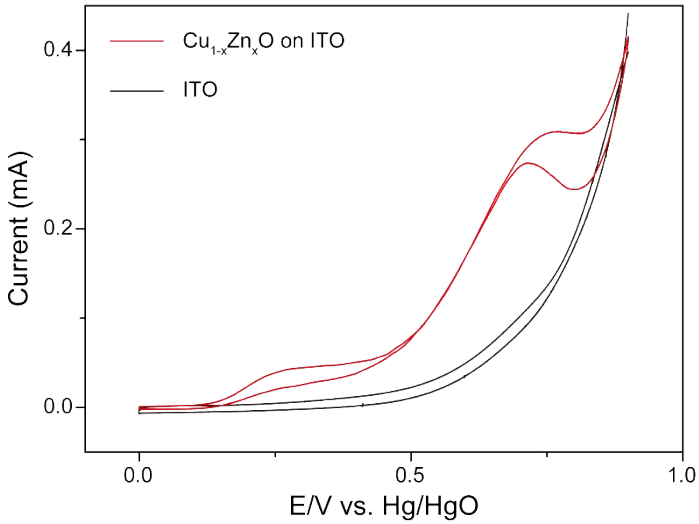

Figure S21. CVs of the bare ITO glass and $Cu_{1-x}Zn_xO$ alloy nanoparticles on ITO glass.

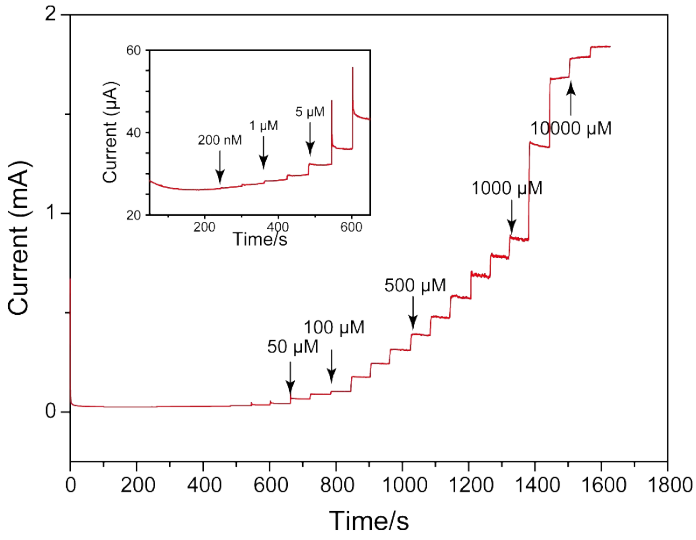

Figure S22. Steady-state amperometric i–t response glucose oxidation at $Cu_{1-x}Zn_xO$ alloy nanoparticles electrode with the successive addition of glucose concentration 50, 100, 500, 1000 and 10000 μM in 0.1 M NaOH. Inset shows amperometric i–t response with the addition of 0.2, 1 and 5 μM of glucose into 0.1 M NaOH. Applied potential, Eapp= +0.75 V.

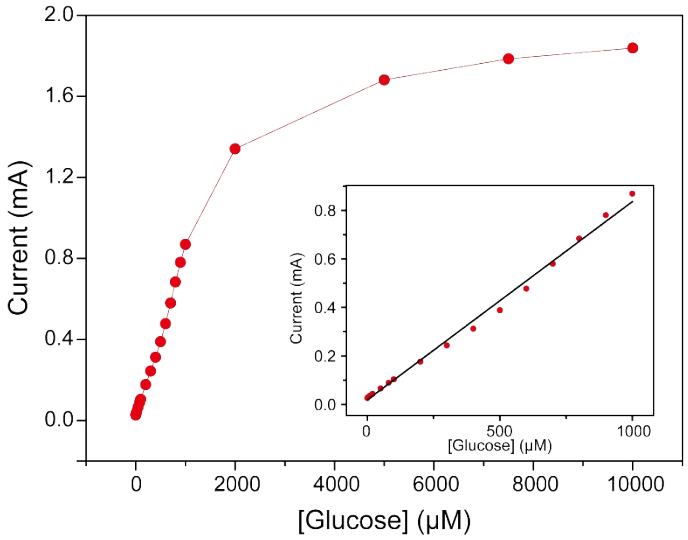

Figure S23. The standard curve of steady-state current responses vs. [Glucose]/μM.

Activated sample	Brunauer-Emmett-Teller (BET) surface area (m^2/g)
HKUST-1-Cu	1701
MTV-HKUST-1-Cu89Zn11	1695
MTV-HKUST-1-Cu78Zn22	1689
MTV-HKUST-1-Cu67Zn33	1676
10%-$Zn(NO_3)_2$-in-HKUST-1-Cu	766
20%-$Zn(NO_3)_2$-in-HKUST-1-Cu	12
30%-$Zn(NO_3)_2$-in-HKUST-1-Cu	4
HKUST-1-Zn	0

Table S1. Surface area of MOF precursors calculated according BET theory.

Sample	Zn^{2+} content based on metal in synthesis (%)	Zn^{2+} content based on metal in product from AAS (%)
MTV-HKUST-1-Cu89Zn11	60	11.27±0.35
MTV-HKUST-1-Cu78Zn22	70	22.54±0.52
MTV-HKUST-1-Cu67Zn33	80	33.96±0.44
10%$Zn(NO_3)_2$-in-HKUST-1-Cu	10	9.57±0.84
20%$Zn(NO_3)_2$-in-HKUST-1-Cu	20	20.96±0.94
30%$Zn(NO_3)_2$-in-HKUST-1-Cu	30	31.24±0.54
PM-HKUST-1-Cu90Zn10	10	11.47±0.42
PM-HKUST-1-Cu80Zn20	20	19.92±0.22
PM-HKUST-1-Cu70Zn30	30	29.86±0.41

Table S2. Zinc amount as determined by AAS.

References

S1. K. Okada, R. Ricco, Y. Tokudome, M. J. Styles, A. J. Hill, M. Takahashi and P. Falcaro, *Adv. Funct. Mater.*, 2014, **24**, 1969-1977.